

Experimental Investigation On The Effects Of The Trw Two Stage Coal Combustor On The Performance Of The Avco Mkvi MHD Generator

Author(s): A. McClaine, J. Pinsley, and B. Pote

Session Name: Topping Cycle

SEAM: 27 (1989)

SEAM EDX URL: <https://edx.netl.doe.gov/dataset/seam-27>

EDX Paper ID: 1316

EXPERIMENTAL INVESTIGATION ON THE EFFECTS OF THE TRW TWO-STAGE* COAL COMBUSTOR ON THE PERFORMANCE OF THE AVCO Mk VI MHD GENERATOR

Andrew McClaine and Judith Pinsley
Avco Research Laboratory, Inc.
Everett, MA 02149

Bruce Pote
Applied Technology Division
TRW Space and Technology Group
Redondo Beach, CA 90278

ABSTRACT

Coal-fired MHD power train testing at the Department of Energy's Component Development and Integration Facility (CDIF) in Butte, MT has resulted in different generator performance (power) than corresponding tests with the ash injected oil-fired combustor. This observation has led to an experimental investigation in the Avco Mk VI MHD Generator Test Facility using engineering prototypes of the 50 MW_t hardware tested at the CDIF.

The objective of the experimental investigation is to resolve the differences between coal and oil-fired operation in terms of the fundamental factors which influence power train performance. Various test hardware configurations and operating conditions have been investigated to understand the role of the coal-fired combustor (CFC) second stage on generator performance. Experiments have included:

- Comparison of performance with single stage versus two-stage combustion
- Modifications to the CFC second stage configuration

Tests using the oil-fired combustor coupled to the CFC second stage have demonstrated that sufficient second stage mixing length is necessary for the two stage combustor to achieve channel power similar to that of the single stage system. Inadequate second stage mixing length resulted in incomplete mixing and combustion, creating lower plasma conductivity and higher plasma non-uniformity. Increasing the second stage mixing length improved the plasma conductivity and reduced non-uniformities resulting in power train performance similar to or better than the bench mark single stage combustor. The results of this ongoing investigation are reported and analyses of experimental data are presented which isolate plasma conductivity and plasma non-uniformity as the primary influences on the measured performance of the generator. Current leakage through the slag layer does not impact generator performance in the magnitude necessary to explain the differences in performance experienced at the CDIF.

INTRODUCTION

In preparation for the Integrated Topping Cycle demonstration, it is necessary to resolve and understand the differences in MHD generator performance (power) observed when the 50 MW_t ash injected oil-fired combustor was replaced with the 50 MW_t coal-fired combustor at the CDIF in Butte, MT. An integrated approach to this task has been taken and is centered around an experimental test program conducted in the Avco Mk VI MHD Generator Test Facility in Everett, MA using the Avco 20 MW_t ash injected combustor (AIC) and the TRW 20 MW_t workhorse coal-fired combustor (CFC). This investigation is augmented by two additional test programs; the 50 MW_t coal-fired power train tests at CDIF and the cold flow modeling activities ongoing at TRW, which are being presented in companion papers.

After careful review of the forcing functions on power output from MHD generators, it became evident that a significant performance upgrade could be realized through optimization of selected aspects of the combustor and channel design. The three primary parameters which dictate power output - plasma conductivity, voltage drops, and current leakage - are highly sensitive to the design and operation of both the combustor and the channel. Additional details on the factors which influence power output can be found in Ref. 1.

The results reported in this paper have focused on the impact of the CFC second stage on the overall generator performance. The paper begins with a brief description of the experimental test logic and hardware. A summary of the operating conditions and measured generator performance follows, which also provides an overview of the conclusions. Comparisons of specific data are presented in the data correlation section to demonstrate the role of the second stage on the overall performance of the generator. These comparisons are drawn between load line data and are supplemented by correlations of power, heat loss and conductivity. Finally, a comparison of the calculated non-uniformity factor is presented which demonstrates the role of plasma non-uniformity on the performance of the generator. From the data correlations, a set of conclusions is proposed to suggest how CDIF performance can be improved through changes in the second stage mixing length.

*This work was sponsored by the U.S. Department of Energy under Contract No. DE-AC22-87PC90274.

Test Logic

Figure 1 summarizes the test logic for the experiments performed in preparation for a comparison between coal-fired operation and oil-fired operation. These tests allowed the impact of the second stage to be separated from the influences of coal versus oil combustion. The ash injected combustor (AIC) is an engineering prototype of the 50 MW_t combustor used at the CDIF. For the initial test sequence, the generator was operated without ash injection.

Single stage combustion in the AIC is considered to be the reference bench mark when making comparisons to alternative configurations and operating conditions. In this baseline test, the AIC was directly coupled to the nozzle assembly in a configuration referred to by its second stage geometric length to diameter ratio of zero ($L/D = 0$).

In the second test series the AIC was again operated as a single stage combustor with the CFC second stage attached in a configuration referred to as $L/D = 2.3$. The addition of the second stage duct effectively increased the combustor residence time since no additional reactants were introduced into the second stage. The purpose of this test was to determine the impact of the second stage duct, separate from the second stage combustion, on generator performance.

In the next test series, the AIC and second stage were operated as a two stage combustor with oxygen enriched air and seed introduced into the AIC portion of the combustor at a nominal first stage stoichiometry of 0.6. The remaining oxidizer in the form of high pressure pure oxygen was introduced into the second stage through the non-impinging oxygen injector frame, providing an overall stoichiometry of 0.95 - 1.0. This two-stage test series addressed the effect of two-stage combustion. The second stage configuration (mixing length) was similar to that used during recent coal-fired testing at CDIF. The configuration was defined by its $L/D = 1.4$ and by a mixing length to height ratio (L/H) of 0.7. The subsequent two-stage test series used a longer second stage configuration ($L/D = 2.3$, $L/H = 2.5$) to evaluate the impact of second stage mixing length.

The absence of ash injection, in addition to providing reliable flow train conditions, removed slag layer leakage from the other influences to the generator performance. The test sequence shown in Figure 1 (except the short mixing length) was therefore repeated with ash injection to verify the trends obtained and to assess the impact of ash injection on generator performance. Again, the bench mark configuration was the AIC operated in a single stage mode coupled directly to the nozzle (second stage $L/D = 0$).

The second phase of the program involves powering the channel with the TRW 20 MW_t coal combustor system. The system consists of an oil-fired vitiator for gas preheat to $\approx 1200^\circ\text{F}$, a coal-fired precombustor for further gas

preheat to $\approx 2900^\circ\text{F}$, the nominal 20 MW_t first stage combustor (slagging stage), the second stage combustor and the Mk VI nozzle, channel and diffuser assembly. The specific focus of the second phase of the program is to compare the oil-fired performance of the generator to the performance of the full coal-fired combustor system, and to optimize the second stage design for coal-fired operation. Optimization of the second stage design will encompass oxidizer injector configuration, hydraulic diameter, and combustion residence time. In addition, the effect on the coal combustor performance due to slag chemistry and seed injection methods will be evaluated. At the time of this writing the Mk VI facility is being converted to coal-fired operation. The results of the coal-fired testing will be presented in future symposia.

HARDWARE DESCRIPTION AND CONFIGURATION

The hardware used during the Phase 1 testing is rated at a nominal 20 MW_t input and is the engineering prototype of the 50 MW_t hardware used at CDIF Test Facility. The power train consists of the following major subsystems; Ash-injected oil combustor (AIC), CFC second stage, and MHD Generator (supersonic nozzle, MHD channel, magnet and diffuser).

Ash Injected Oil Combustor (AIC)

The AIC is a highly turbulent, circular cross-section (Dia. = 23 cm) burner characterized by excellent fuel atomization and mixing. These characteristics are obtained through high pressure drop injection of the fuel and oxidizer. Coaxial fuel/oxidizer injectors are located circumferentially around the injector ring and oriented radially to promote turbulent mixing in the combustion chamber. High pressure injection of the ionizing seed (K_2CO_3) with the oxidizer promotes uniform dispersion and rapid ionization of the potassium. Ash particles (as appropriate) are injected through the combustor back plate to simulate the mineral matter contained in coal. For these tests, the ash was a Western Ash collected from a power plant operating on a Montana Rosebud coal. Typical combustor residence time was on the order of 10 milliseconds.

CFC Second Stage

The second stage combustor consists of individual water cooled copper frames of rectangular cross-section, nominally 13.5 cm x 23.0 cm. The walls of each section are grooved to promote slag retention. This second stage is normally operated in conjunction with a coal-fired slagging first stage. Two second stage configurations were evaluated during the experimental investigation. They are shown connected to the AIC burner and nozzle, in both the plan and side views in Figures 2 and 3. Figure 2 shows the layout with the short second stage. It has an overall length to hydraulic diameter (L/D) of 1.4 and mixing length to height (L/H) of 0.7. Similarly, Figure 3 shows the layout with the long second stage for an overall L/D of 2.3 and a mixing L/H of 2.5. When the second stage was operated with oxygen injection, a

non-impinging oxygen injector, oriented counter flow to the plasma flow as shown in Figure 4, was used. Non-impinging implies that the jets on opposite sides do not intersect with one another. For these tests, oxygen was injected along the top and bottom walls (electrode wall injection) using either a total of 8 or 12 injectors. The 8 port injector scheme was accomplished by valving off the outside two injectors on both the top and bottom. Injector diameter could be varied by the use of injector inserts, but unless noted only 0.635 cm diameter injectors were utilized.

MHD Generator

The MHD generator consists of four major assemblies; the nozzle, the MHD channel, the magnet, and the diffuser.

The supersonic nozzle is made of individual water cooled copper frames that accelerate the plasma to a nominal inlet Mach Number of 1.2.

The Mark VI MHD generator is made of four separable walls which form a duct of rectangular cross section and contains 149 electrode pairs with an electrode pitch of 1.78 cm. The overall length of the channel is approximately 250 cm. It has an exit to inlet area ratio over the loaded region of 3.11. There are 112 active electrodes in the loaded portion of the generator. The channel is operated in the pure diagonal mode with an overlap of twelve electrodes ($n + 12$) operated with current control circuitry. The channel is connected to externally adjustable resistive loads which range from short circuit to open circuit conditions. Individual electrodes are water cooled copper and are clad with various corrosion resistant metals on the gas side surfaces. Inter-electrode insulators are boron nitride. The insulating sidewalls are constructed of water cooled copper pegs with interpeg insulators of boron nitride. The insulating sidewalls effectively stand off both the Faraday and Hall electric fields.

The MHD channel sits inside the bore of a copper coil, iron core electromagnet powered by variable dc rectifiers. For this program, tests were performed at a peak magnetic field of 3 Tesla.

The diffuser consists of both supersonic and subsonic sections for efficient recovery of the exhaust stream to atmospheric pressure prior to entering the quench, gas cleaning and exhaust stack.

SUMMARY OF TEST CONDITIONS AND GENERATOR PERFORMANCE

Summary of Test Conditions

Tests were conducted with and without ash injection. Specific input conditions for the tests described in subsequent sections are summarized in Tables 1 and 2, for the no ash and ash tests, respectively.

Summary of Generator Performance

Figure 5 shows a plot of peak power as a function of test hardware conditions. The plot demonstrates how the power has been nearly restored to the single stage reference through judicious changes in the second stage configuration. Moving from left to right across the plot, the initial drop in power associated with the addition of the second stage duct, as will be shown later, is primarily due to the additional heat loss caused by the added combustor wall area. The subsequent drop in power associated with the two stage configuration ($L/H = 0.7$) demonstrated a qualitatively similar decrease in performance as that experienced at CDIF. Increasing the second stage mixing length and providing adequate jet spatial distribution (8 vs. 12 port) nearly restored the power to the single stage value.

Plotting the open circuit voltage in Figure 6 for the same cases further demonstrates the role of second stage mixing length on generator performance. The simple addition of the second stage duct did not have a significant effect on open circuit voltage. However, the short duct operating in a two-stage mode showed a 30 percent drop in open circuit voltage which is similar to that experienced at CDIF. This drop in open circuit voltage cannot be attributed to slag layer leakage since these tests were conducted with bare walls. Increasing the mixing length restores the open circuit voltage to values similar to the single stage condition. These results suggest that second stage mixing may be the primary cause of the decrease in generator power experienced at the CDIF.

Figure 7 shows a plot of the peak power obtained for various configurations with ash injection, exhibiting a similar trend to that obtained without ash injection. The drop in power with the addition of the second stage duct is due to the expected increase in total combustor heat loss. The power is restored to the nominal single stage level during two-stage operation ($L/H = 2.5$) when the 12 port injector scheme is used. In fact, the two-stage performance actually exceeded that of the reference single stage ($L/D = 0$). A small (arguably insignificant) improvement was also obtained when the injector diameter was increased by approximately 12 percent. In this case, an improvement in jet spatial distribution is achieved at the expense of oxygen injection velocity. Essentially, the open circuit voltage was unchanged throughout the ash test series and was of similar magnitude to the no ash test. One explanation for this latter observation is that there is not a significant current leakage associated with the slag layer.

DATA CORRELATIONS

Data Analysis Techniques

The MHD generator has proven to be an accurate indicator of combustor effectiveness. One of the most powerful diagnostic techniques has been the analysis of the measured load

line. It has been shown in Refs. 2 and 3 that a reduction in short circuit current is caused by a reduction in plasma conductivity, and that a reduction in open circuit voltage can be caused by an increase in current leakage. A simultaneous reduction in both the short circuit current and open circuit voltage might be caused by a combination of a current leakage and a conductivity drop, by an increase in the voltage drop or by an increase in plasma non-uniformity. These effects have been predicted by simplified models such as those outlined in Refs. 2 and 3, and through the use of the Avco MHD4 performance prediction code. The latter model is a more rigorous quasi one-dimensional model which combines electrical and fluid dynamic properties to predict generator performance.

In the following discussion, comparisons of load lines will be made to determine whether hardware and operation changes are causing changes in the open circuit voltage, the short circuit current or both. Load lines measured during tests in which the generator was configured with the ash injected combustor with no second stage duct will be used as the reference bench mark. Results from subsequent hardware and operation changes will be compared to the bench mark condition to determine the effects on generator performance.

Effect of Second Stage Duct Length

Figure 8 displays the load lines measured with no second stage and with a second stage configured for a L/D ratio of 2.3, with no oxygen injection. The error bars define one standard deviation from the mean for the time averaged data. Two of the load lines display the performance of the generator at the nominal operating condition. The third line displays the performance of the generator, with the second stage duct, at a condition for which fuel was added to partially compensate for the second stage duct heat loss. The reduction of the short circuit current at the nominal condition indicates that the heat loss of the second stage duct reduced the plasma conductivity. However since the open circuit voltage is the same both with and without the second stage duct, then the mere presence of the duct must not be responsible for additional axial current leakage or increased voltage drops which are potential causes of the observed power shortfall.

Two Stage Versus Single Stage Combustion and Second Stage Mixing Length

Figure 9 and Figure 10 display the load lines for two-stage combustion using the short and long second stage, respectively. In both cases, the two-stage performance is plotted against the reference single stage condition ($L/D = 0$). With the short second stage mixing length the performance of the generator is significantly reduced with respect to the baseline condition. A reduction in open circuit voltage of 30 percent and a reduction in short circuit current of 25 percent were realized. This decrease in generator performance was similar to

that observed at the CDIF when the oil fired combustor was replaced with the coal fired power train Ref. 1. The reduction in open circuit voltage cannot be associated with slag layer leakage since the tests were conducted bare wall. The reduction in V_{oc} and I_{sc} could be caused either by a plasma non-uniformity or by an increased voltage drop along with reduced conductivity resulting from inadequate mixing and combustion in the second stage.

The importance of second stage mixing length and residence time is demonstrated by the results of the test with the longer second stage shown in Figure 10. With the increased mixing time (mixing length was increased by a factor of 3.5), the open circuit voltage and power were significantly improved with respect to the reference baseline condition. The slightly lower open circuit voltage and lower short circuit current of the two-stage test compared to the reference condition could be explained by differences in the characteristic voltage drops for the different channels used and the higher component heat losses for the two-stage test. The latter resulted from the gradual degradation in the castable refractory used to protect gas side surfaces. The improvement in generator performance resulting from an increase in the second stage mixing length suggests that plasma non-uniformities introduced by the second stage can be minimized by optimization of the second stage design.

Effect of Jet Spatial Distribution

Figure 11 compares the load lines for the 12 port and 8 port injector configurations with the short second stage. With the short second stage mixing length, the open circuit voltage and short circuit current were both further reduced as the number of oxygen ports was reduced. This result suggests that the performance of the generator is sensitive to the number of oxygen jets (spatial distribution) when the available mixing length is minimized, as this produces additional spatial non-uniformities that degrade generator performance. Figure 12 compares similar 12 and 8 port data for the long second stage mixing length configuration. The reduction in generator performance was not appreciable with the long mixing length when the number of injectors was reduced. The mixing and combustion residence time in the long second stage is sufficient to overcome the inadequate oxidizer mixing scheme caused by the 8 port configuration. This may suggest that a small decrease in the second stage mixing length with 12 ports could be tolerated in order to reduce the heat loss without a degradation in generator performance due to mixing non-uniformities.

Effect of Ash Injection

A similar set of comparisons was made for slag covered walls as was made for bare walls. The baseline case was configured with the AIC operated single stage with ash injection. The load line measured with the long second stage duct, operated as a single stage combustor, showed a reduction in the short circuit current

due to the increased combustor heat loss. No decrease in the open circuit voltage was noted. This result corresponded to the bare wall tests.

Figure 13 displays the comparison of single stage ($L/D = 0$) versus two stage ($L/D = 2.5$) combustion. The two stage test with adequate mixing length performs better than the single stage run. Since the same trend was observed with bare walls, this implies that the simple addition of ash does not degrade the performance of the power train, and suggests that slag layer leakage is not responsible for the power shortfall experienced at CDIF.

In the past, ash carry-over rate has also been suspected as a major cause for reduced open circuit voltage. This was not a possible explanation for the bare wall observations because the tests were performed without ash injection. However, the ash carry-over rate has been observed to affect the open circuit voltage in the Mk VI ash injection tests. Figure 14 displays the comparison of the load current versus the load voltage for a 10 percent carry-over rate and a 30 percent carry-over rate. A slight decrease in the load voltage as the ash carry-over rate is increased can be noted in the figure. Also the number of opens is found to decrease as the carry-over rate is increased. These effects are noticeable but are not of a magnitude to explain the power shortfall. Figure 14 also compares the bare wall to the slagged wall data. Open circuit voltage was found to be comparable. On first consideration this would appear to imply that there was no increase in the current leakage. While this may be true, it is also possible that the increased wall temperature has reduced the voltage drop, giving the slagged wall load line a parallel shift upward. At the same time an increased current leakage has reduced the open circuit voltage to its original value.

Conductivity Correlation

Figures 15 and 16 display correlations of the measured bulk conductivity with the combustor heat loss and the peak power calculated from the bare wall loadlines. Bulk conductivity is calculated from the power supply current, the sum of the inter-anode voltages, and the mid-channel cross-sectional area. The case letters are identified in Table 1. These figures can be used to differentiate between performance differences caused by heat loss in the combustor, differences caused by the injector/mixing scheme (improved combustion) or non-uniformities in the channel.

In Figure 15, two trends are observed, one relating measured conductivity to combustor heat loss (cases C, A, M, and O) and the other independent of combustor heat loss (cases K and G). Cases K and G have lower overall heat losses than the other cases but do not generate the expected plasma conductivity. This suggests that a parameter other than heat loss is reducing the conductivity. Cases K and G represent the combustor configured with the short second stage duct. The increase in conductivity of case G, at a similar heat loss as case K, is

due to the improvement in the mixing scheme (12 port vs. 8 port) and hence, improved combustion. Even with the improved mixing scheme, though, case G still does not generate the expected plasma conductivity for the measured heat loss, implying that the mixing length is inadequate. Assuming perfect mixing and ignoring any limitations due to reaction kinetics, the expected conductivity for the combustor configured with the short second stage should approach 5 mho/m. The direct relationship between conductivity and heat loss for the baseline and long mixing length cases C, A, M, and O suggests that combustion is complete in those configurations.

Figure 16 is a plot of the peak output power as a function of the measured conductivity. The data fall into two families of curves. The results for cases G and K (short duct) generate one data set while the results for the reference configuration (case C) and the test cases with the long second stage form another. The power increase achieved by increasing the number of second stage oxygen injector (case G vs. K) was proportional to the increase in measured conductivity. However, case G makes 50 percent of the power of the reference single stage condition (case C) at the same value of plasma conductivity. This suggests that the short mixing length has created a nonuniformity in the plasma which causes a performance shortfall. A similar trend has been observed at the CDIF where power increases have been proportional to conductivity increases. For the same measured conductivity, however, the CFC still produced less power than the AIC (Ref. 1).

The second curve is shown drawn through the reference condition (case C). The data for the other test cases fall around this power-conductivity correlation. The drop in conductivity from case C to case A was due primarily to the additional heat loss of the second stage duct as shown in Figure 15. However, case A does not make the expected power relative to the reference case. Cases M and O show the performance of the two stage combustor with the long mixing length configuration. They use 12 and 8 injector ports, respectively. Cases M and O make higher power relative to the reference case and further demonstrate the importance of the second stage mixing scheme. One can speculate that if the combustor heat losses could be reduced for cases M and O, then the peak power would exceed that of the single stage baseline condition.

The results for cases C, A, M, and O show that conductivity correlates directly with heat loss while power vs. conductivity is not directly proportional. This implies that small differences in plasma non-uniformity exist for the test cases M, O, and A relative to the baseline (cases M and O may be more uniform, case A may be less uniform), which result from a parameter other than inadequate mixing length.

Non-Uniformity Correlation

Another technique for evaluating the performance of the generator is to compare the

degree of plasma non-uniformity for the various test cases. Higher values of non-uniformity result in a degradation in the power output. A variable G-factor has been defined by Rosa (Ref. 5) to account for this non-uniformity by modeling it as alternating layers of high and low conductivity in the core flow. By calculating the magnitude of the non-uniformity factor under various operating conditions, an overall measure of combustor performance may be inferred. The non-uniformity factor (G-factor) can be determined from the global generator conditions, assuming zero link resistance, as follows:

$$I_{sc} = \frac{\sigma u A B (1-\Delta)(\tan \theta + \beta)}{G + \beta^2} \quad (1)$$

$$\Delta = \frac{\Delta V_{bl}}{u B H} \quad (2)$$

$$\tan \theta = \frac{NP}{H} \quad (3)$$

where:

I_{sc}	is the short circuit current
σ	is the bulk conductivity
u	is the average plasma velocity
A	is the cross-sectional area
B	is the magnetic field strength
β	is the Hall parameter
G	is the non-uniformity factor which varies between 1 and infinity
N	is the number of overlapped electrodes determined by the diagonal connection angle
P	is the electrode pitch
H	is the channel height
ΔV_{bl}	is the boundary layer voltage drop

After substituting and rearranging and assuming a constant u and β , the following relationship is obtained:

$$\frac{I_{sc}}{\sigma(1-\Delta)} \propto \frac{1}{G + \beta^2} \quad (4)$$

Since β is nearly constant for the various test conditions the relationship of I_{sc} , σ , and $(1-\Delta)$ (which are measured parameters) goes as the inverse of the non-uniformity factor G . Higher values of $1/(G+\beta^2)$ imply low non-uniformity and hence better mixing.

Through this relationship, the G-factor is isolated from the effects of voltage drop, heat loss, and conductivity. Slag layer leakage is absent in the no ash tests, so only the G-factor can explain differences in generator performance. Figure 17 shows the relationship of the G-factor correlation to the various test cases for no ash injection. Case A has a higher non-uniformity factor than the reference condition, which explains why the power, as shown in Figure 16, is below expectations based on the measured conductivity. A significant increase in non-uniformity is observed with the short duct tests which reiterates the importance of mixing length. Case M has a lower

non-uniformity factor which supports the speculation that, at the same conductivity as case C, case M would generate more power than the reference condition.

Figure 18 shows the relationship of G-factor for the corresponding test cases with ash injection. The trend observed is identical to the power trend illustrated in Figure 7. The remarkably consistent proportionality constant between the power and the non-uniformity factor for the ash injection tests is further evidence that the power shortfall is due to non-uniformities caused by the second stage. Only through optimization of second stage parameters (primarily second stage mixing length) are the power and G-factor restored to the bench mark single stage value.

CONCLUSIONS

The 20 MW_t two-stage combustor, without ash injection, results in performance degradation similar to that observed with the coal-fired combustor at CDIF. Based on the data collected in the Mk VI facility using the Avco AIC coupled with the TRW CFC second stage, poor second stage mixing (injector configuration and mixing length) and insufficient residence time can contribute to substantial plasma nonuniformities entering the channel. These non-uniformities result in a reduced plasma conductivity and power output. The plasma conductivity and power can be improved substantially by increasing the second stage length and optimizing the injector spatial distribution. These are the primary parameters which can be optimized to improve CDIF generator performance.

This conclusion has been drawn from comparisons made for the peak power generated, the load voltage, the short circuit current, the measured conductivity, combustor heat loss and plasma non-uniformity under conditions of no ash and ash injection.

Slag layer leakage also has been suggested as a cause of the reduced performance at CDIF. In the tests conducted at Avco, a similar performance trend (reduced open circuit voltage) was observed when no slag layer existed. In the subsequent slagging tests, slag layer leakage was shown to have a small effect on the open circuit voltage but contributed to an increase in power due to the thermally insulating barrier formed on the power train walls.

The most notable comparisons are between the short mixing length data and the long mixing length data. Performance and non-uniformity parameter comparisons conclude that the long mixing length configuration is preferred. Spatial distribution variations confirm that more injectors provide a more uniform plasma and therefore better generator performance. Correlating power, conductivity, and G-factor trends for each of the configurations implies that better mixing causes higher performance for comparable measured plasma conductivity.

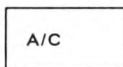
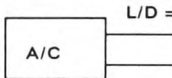
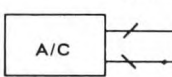
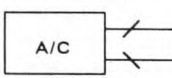
The second phase of this program will focus on confirming these conclusions with the

20 MW_t TRW coal-fired combustor. An optimization of the second stage configuration to maximize the mixing while minimizing heat loss will be determined.

References

1. Braswell, R., Grove, A., Pote, B., "Coal-Fired MHD Power Train Performance Upgrade Test Activities," 27th Symposium of Engineering Aspects of MHD, Reno, NV, June 1989.
2. Avco Research Laboratory, Inc., "MHD Channel Development," Quarterly Progress Report, Contract No. DE-AC22-84PC70507, July 1986, pp. 7-30.
3. Pian, C.C.P., Petty, S.W., McClaine, A.W., "Operating Characteristics of a Slagging Diagonally-Loaded Magnetohydrodynamic Power Generator," 25th Symposium on Engineering Aspects of MHD, Bethesda, June 1987.
4. TRW Space and Technology Group, Applied Technology Division, "MHD Integrated Topping Cycle," Fourth Quarterly Report Number MHD-ITC-88-133, Contract No. DE-AC22-87PC90274, September 1988, pp. 4-14 through 4-27.
5. Rosa, R.J., "Magnetohydrodynamic Energy Conversion," Hemisphere Publishing Corp., Copyright 1987, pp. 74-78.

TABLE 1
SUMMARY OF INPUT CONDITIONS FOR TESTS WITH NO ASH INJECTION

TEST I.D. CASE	TEST CONFIGURATION	N/O GLOBAL	TOTAL MASS FLOW (LB/S)	SEED (K)	PHI 1	PHI 2	OIL FLOW (GAL/MIN)	OXY.1 FLOW (LB/S)	OXY.2 FLOW (LB/S)	SEED FLOW (LB/MIN)	AIR FLOW (LB/S)	ASH FLOW (LB/MIN)	NUMBER OF INJECTOR PORTS
AA	SINGLE STAGE	1.00	7.10	1.01	-	0.97	8.15	2.28	-	7.3	3.63	1.4	0
AB	 L/D = 0	1.01	7.18	1.00	-	0.98	8.17	2.29	-	7.7	3.52	3.4	0
Y	SINGLE STAGE  L/D = 2.3	0.98	6.86	1.04	-	0.95	8.14	2.31	-	7.8	3.48	2.3	0
R	TWO STAGE L/D = 2.3	1.00	7.03	1.19	0.61	0.97	8.11	1.17	1.06	8.8	3.68	1.4	12
S	 L/D = 2.3 NON-IMP L/H = 2.5	1.03	6.98	1.21	0.61	0.95	8.04	1.12	1.07	9.1	3.67	1.6	8
U	TWO STAGE L/D = 2.3  L/D = 2.3 NON-IMP L/H = 2.5 INJ. DIA. = 0.281"	1.02	7.02	1.19	0.60	0.95	8.07	1.10	1.07	8.8	3.63	2.5	12

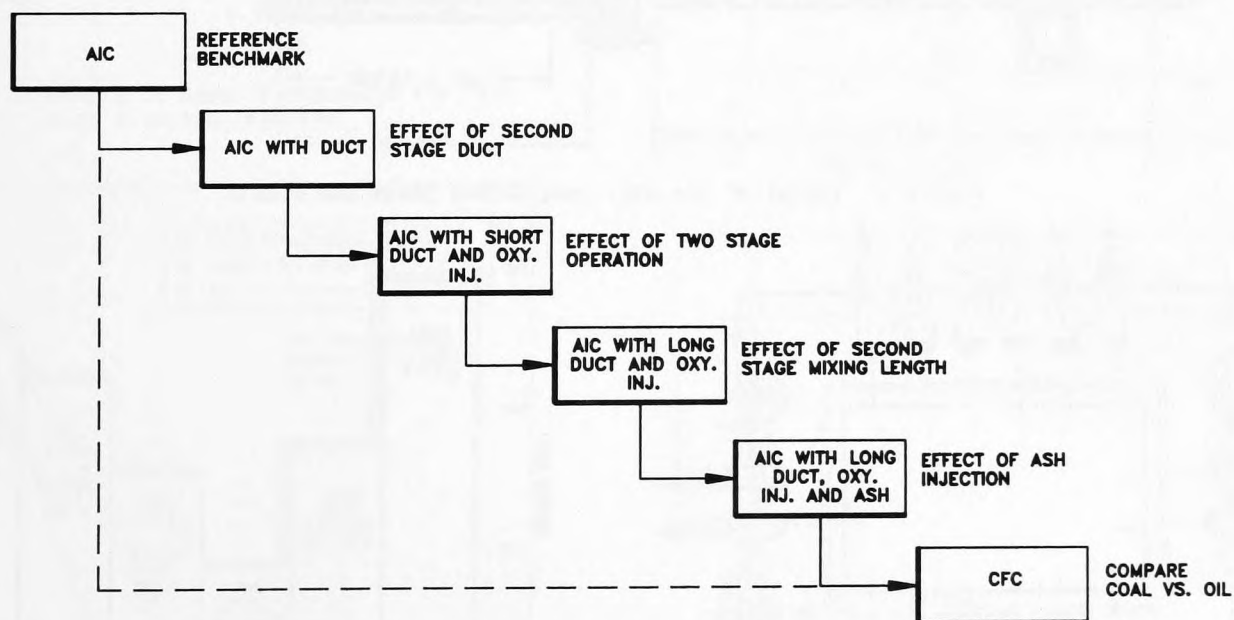
N7262

TABLE 2

SUMMARY OF INPUT CONDITIONS FOR TESTS WITH ASH INJECTION

TEST I.D. CASE	TEST CONFIGURATION	N/O	TOTAL MASS FLOW (LB/S)	SEED (% K)	PHI 1	PHI 2	OIL FLOW (GAL/MIN)	OXY.1 FLOW (LB/S)	OXY.2 FLOW (LB/S)	SEED FLOW (LB/MIN)	AIR FLOW (LB/S)	NUMBER OF INJECTOR PORTS
C	SINGLE STAGE A/C L/D = 0	0.98	6.81	1.06	-	0.95	8.01	2.23	-	7.6	3.44	0
A	SINGLE STAGE A/C L/D = 2.3	1.00	6.81	1.08	-	0.95	7.92	2.14	-	7.8	3.55	0
B	A/C	0.87	6.60	1.10	-	0.95	8.31	2.37	-	8.0	3.17	0
G	TWO STAGE L/D = 1.4	0.98	7.03	1.03	0.64	1.00	7.99	1.20	1.13	7.7	3.60	12
K	A/C NON-IMP INJ. L/H = 0.7	0.97	7.10	1.03	0.64	1.01	8.00	1.23	1.14	7.7	3.61	8
M	TWO STAGE L/D = 2.3	0.98	7.15	1.05	0.64	1.01	7.99	1.20	1.12	8.0	3.73	12
O	A/C NON-IMP INJ. L/H = 2.5	0.97	7.23	1.08	0.65	1.03	7.99	1.26	1.13	8.2	3.72	8

N7263



M9831

Figure 1 Summary of Test Logic

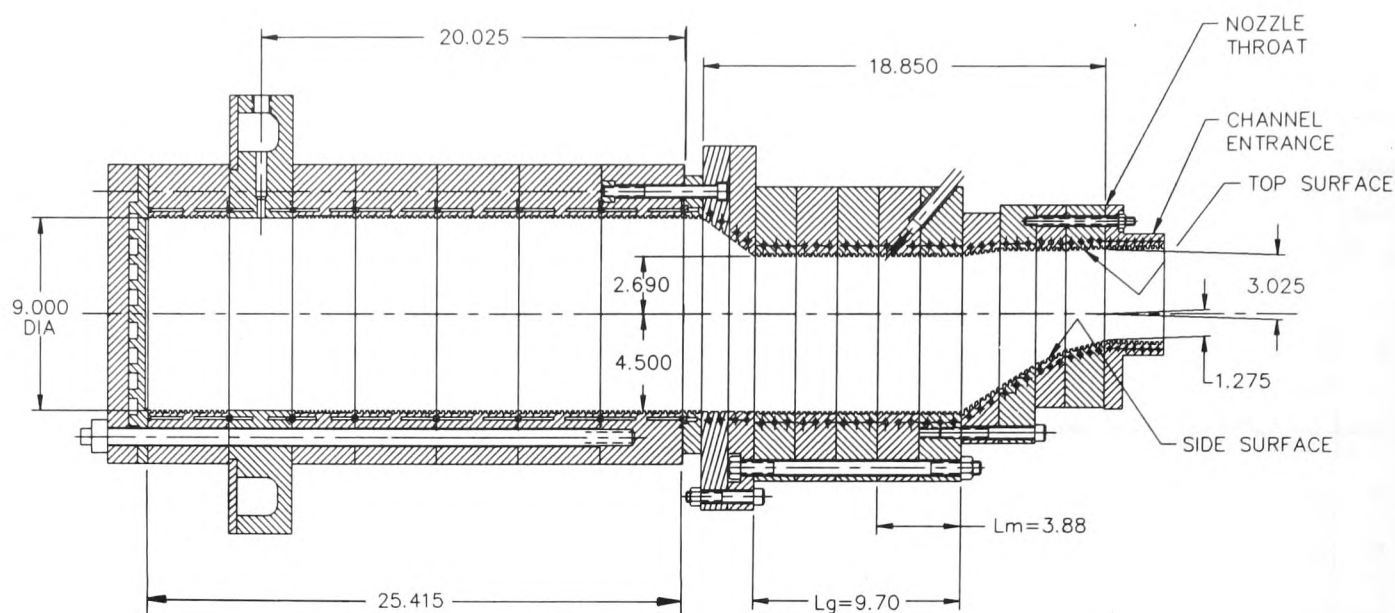


Figure 2 Layout of the AIC, Short Second Stage and Nozzle

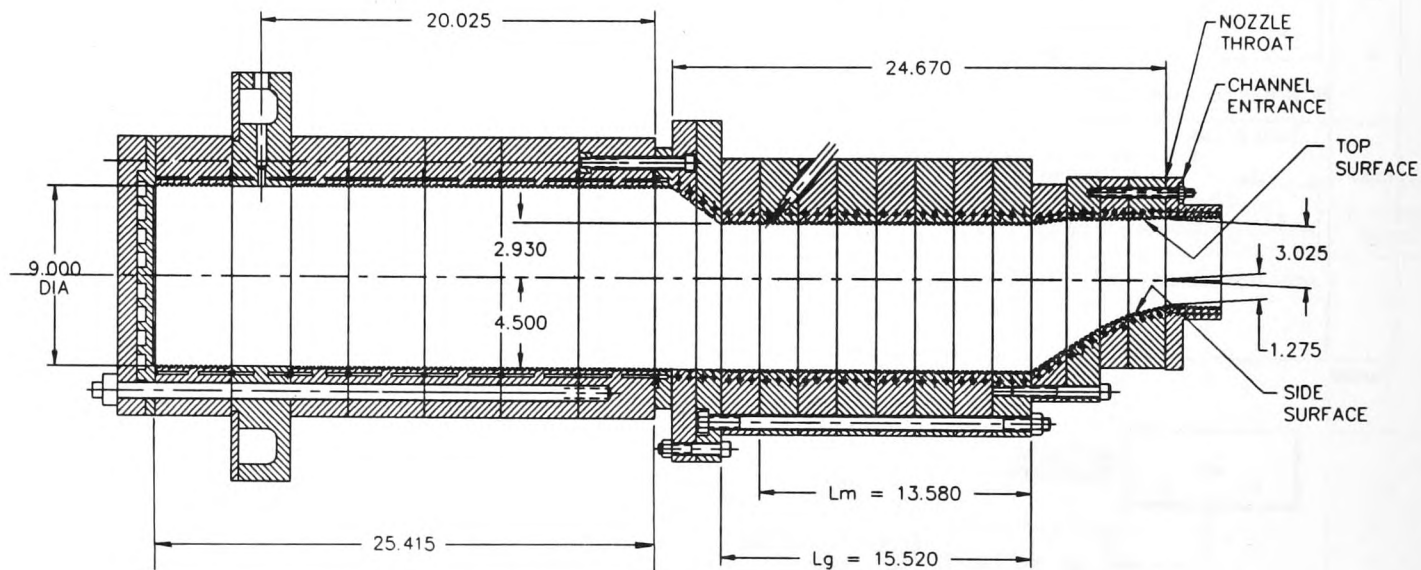


Figure 3 Layout of the AIC, Long Second Stage and Nozzle

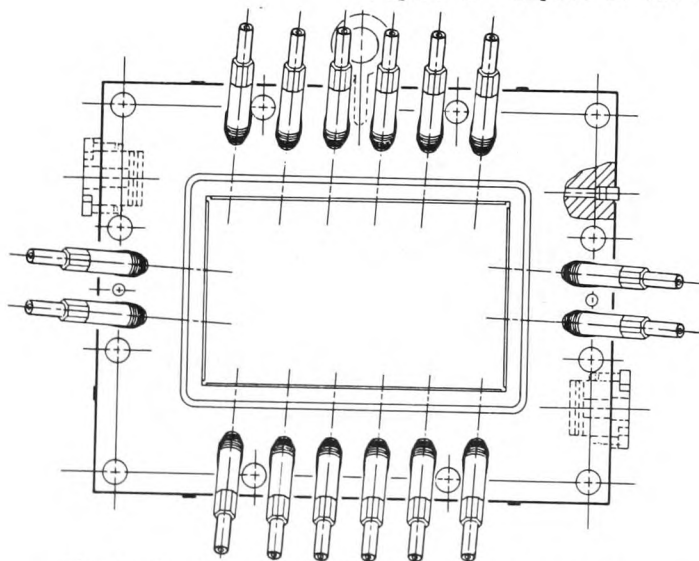


Figure 4 Layout of the Non-Impinging Oxygen Injector Frame

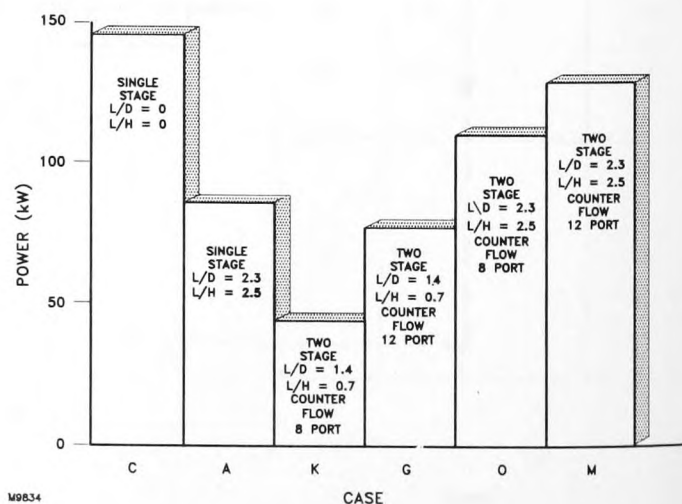


Figure 5 Summary of Power Performance for Test Cases with No Ash Injection

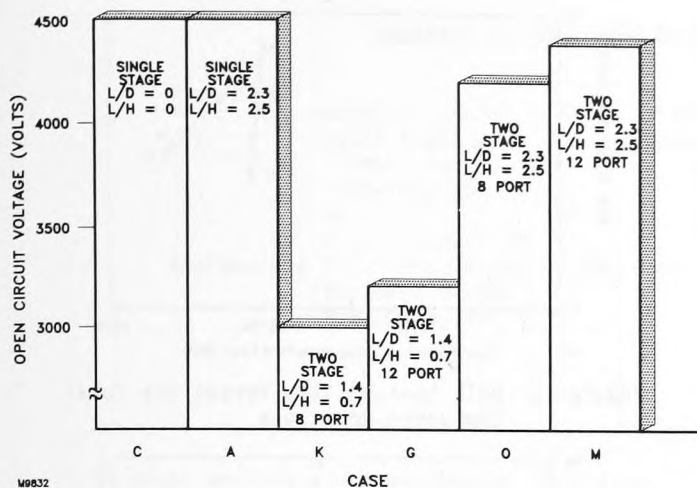


Figure 6 Summary of Open Circuit Voltage for Test Cases with No Ash Injection

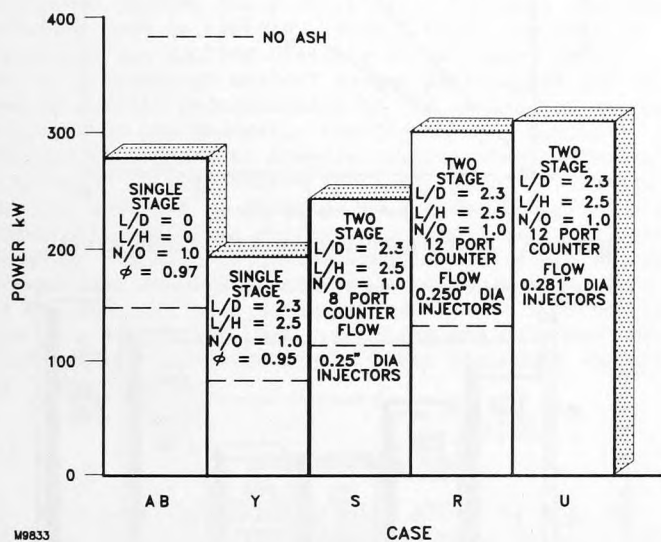


Figure 7 Summary of Power Performance for Test Cases with Ash Injection

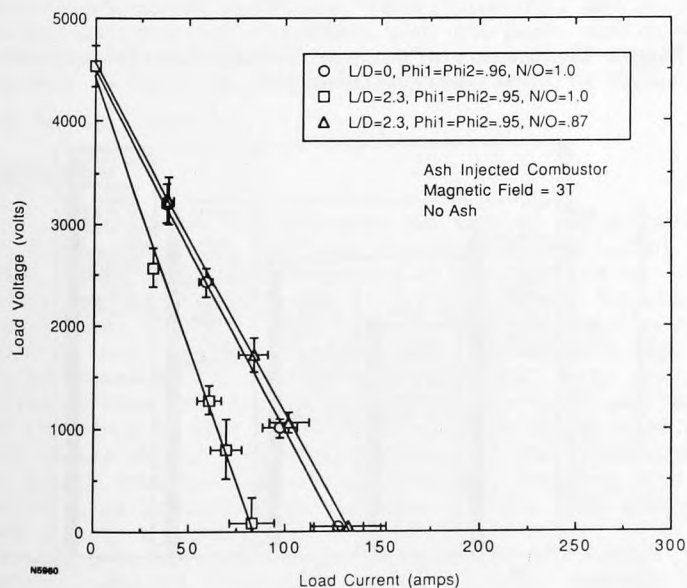


Figure 8 Effect of the Second Stage Duct with Single Stage Combustion

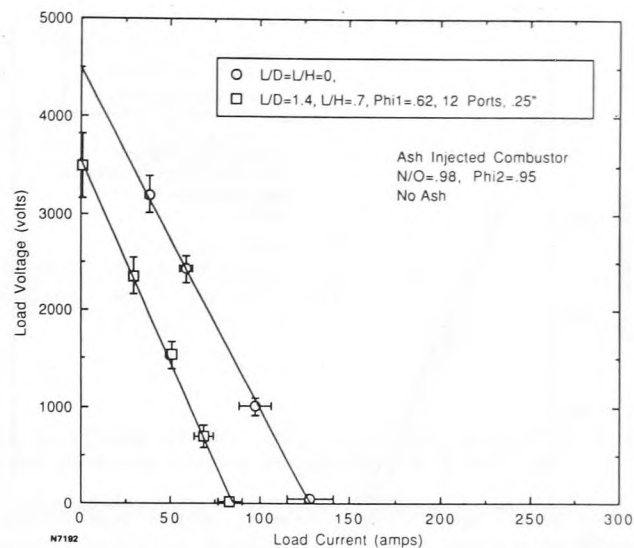


Figure 9 Effect of Two Stage Combustion with Short Mixing Length

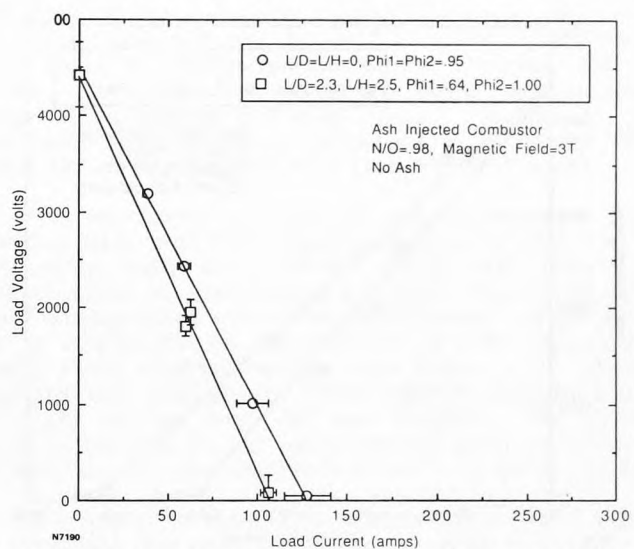


Figure 10 Effect of Two Stage Combustion with Long Mixing Length

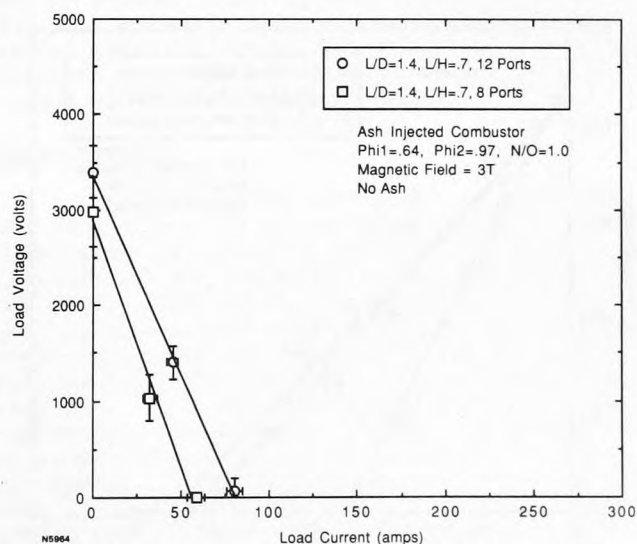


Figure 11 Effect of Spatial Distribution with Short Mixing Length

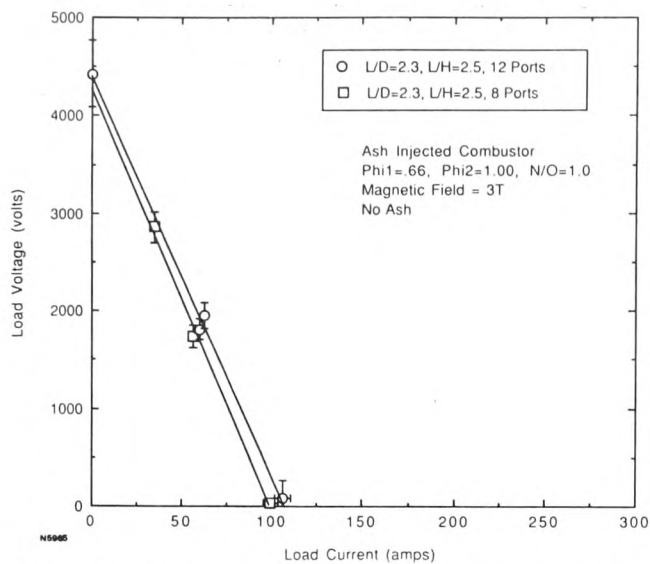


Figure 12 Effect of Spatial Distribution with Long Mixing Length

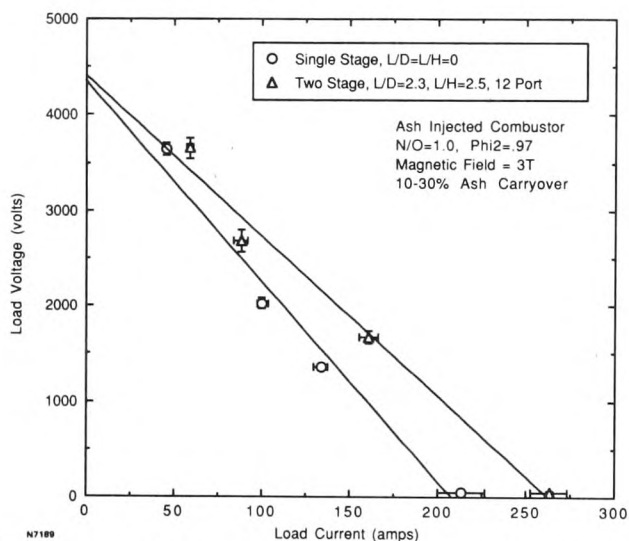


Figure 13 Effect of Two Stage Combustion with Ash Injection

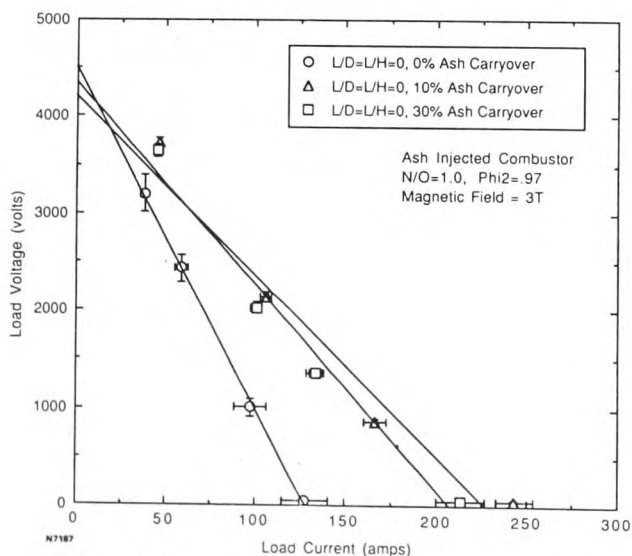


Figure 14 Effect of Ash Carryover Rate

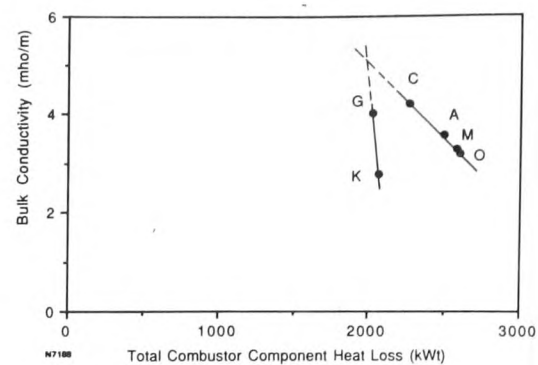


Figure 15 Bulk Conductivity Versus the Total Combustor Heat Loss

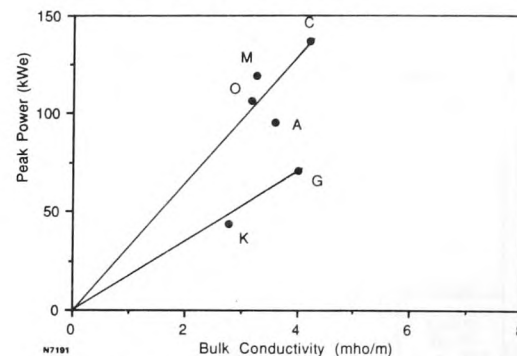


Figure 16 Peak Power Versus Bulk Conductivity

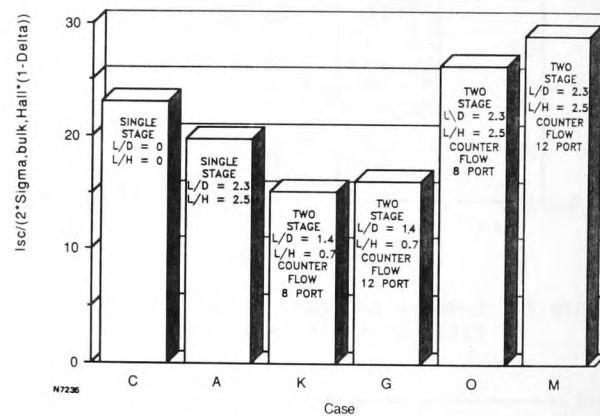


Figure 17 Summary of Non-uniformity Correlation for Test Cases with No Ash

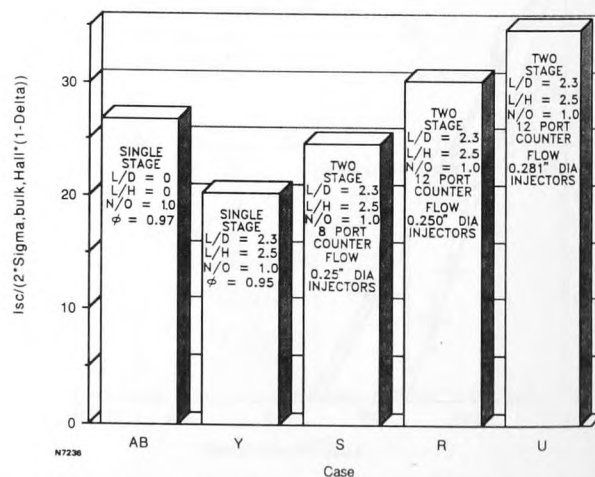


Figure 18 Summary of Non-uniformity Correlation for Test Cases with Ash Injection